Preclinical Characterization of ^{18}F-MK-6240, a Promising PET Tracer for In Vivo Quantification of Human Neurofibrillary Tangles

Eric D. Hostetler[1], Abbas M. Walji[2], Zhizhen Zeng[1], Patricia Miller[1], Idriss Bennacef[1], Cristian Salinas[1], Brett Connolly[1], Liza Gantert[1], Hyking Haley[1], Marie Holahan[1], Mona Purcell[1], Kerry Riffel[1], Talakad G. Lohith[1], Paul Coleman[2], Aileen Soriano[3], Aimie Ogawa[3], Serena Xu[3], Xiaoping Zhang[3], Elizabeth Joshi[4], Joseph Della Rocca[5], David Hesk[6], David J. Schenk[6], and Jeffrey L. Evelhoch[1]

[1]Translational Biomarkers, Merck & Co., Inc., West Point, Pennsylvania; [2]Discovery Chemistry, Merck & Co., Inc., West Point, Pennsylvania; [3]Pharmacology, Merck & Co., Inc., Kenilworth, New Jersey; [4]Drug Metabolism, Merck & Co., Inc., West Point, Pennsylvania; [5]Discovery Pharmaceutical Sciences, Merck & Co., Inc., West Point, Pennsylvania; and [6]Labelled Compound Synthesis, Merck & Co., Inc., Rahway, New Jersey

A PET tracer is desired to help guide the discovery and development of disease-modifying therapeutics for neurodegenerative diseases characterized by neurofibrillary tangles (NFTs), the predominant tau pathology in Alzheimer disease (AD). We describe the preclinical characterization of the NFT PET tracer ^{18}F-MK-6240. **Methods:** In vitro binding studies were conducted with ^{3}H-MK-6240 in tissue slices and homogenates from cognitively normal and AD human brain donors to evaluate tracer affinity and selectivity for NFTs. Immunohistochemistry for phosphorylated tau was performed on human brain slices for comparison with ^{3}H-MK-6240 binding patterns on adjacent brain slices. PET studies were performed with ^{18}F-MK-6240 in monkeys to evaluate tracer kinetics and distribution in the brain. ^{18}F-MK-6240 monkey PET studies were conducted after dosing with unlabeled MK-6240 to evaluate tracer binding selectivity in vivo. **Results:** The ^{3}H-MK-6240 binding pattern was consistent with the distribution of phosphorylated tau in human AD brain slices. ^{3}H-MK-6240 bound with high affinity to human AD brain cortex homogenates containing abundant NFTs but bound poorly to amyloid plaque–rich, NFT-poor AD brain homogenates. ^{3}H-MK-6240 showed no displaceable binding in the subcortical regions of human AD brain slices and in the hippocampus/entorhinal cortex of non-AD human brain homogenates. In monkey PET studies, ^{18}F-MK-6240 displayed rapid and homogeneous distribution in the brain. The ^{18}F-MK-6240 volume of distribution stabilized rapidly, indicating favorable tracer kinetics. No displaceable binding was observed in self-block studies in rhesus monkeys, which do not natively express NFTs. Moderate defluorination was observed as skull uptake. **Conclusion:** ^{18}F-MK-6240 is a promising PET tracer for the in vivo quantification of NFTs in AD patients.

Key Words: tau; neurofibrillary tangles; Alzheimer's disease; PET; ^{18}F

J Nucl Med 2016; 57:1599–1606
DOI: 10.2967/jnumed.115.171678

Currently, the clinical evaluation of disease-modifying therapies for Alzheimer disease (AD) requires large, resource-intensive clinical trials focused on measuring cognitive endpoints, which are highly variable. A biomarker that could be used early in clinical development to build confidence in the ability of a therapeutic mechanism to modify disease progression would provide a valuable bridge to investment in a large efficacy study once adequate pharmacokinetics, safety, and tolerability have been established. Biomarkers currently in use (e.g., volumetric MRI, amyloid plaque PET, cerebrospinal fluid measures of amyloid-β and tau) either do not directly inform on modification of disease pathology (volumetric MRI) or do not correlate strongly enough with cognitive decline to measure therapeutic response (amyloid plaque PET and cerebrospinal fluid measures) (*1,2*). Therefore, there is an unmet need for sensitive biomarkers that quantify early pathologic changes and correlate closely to disease progression and clinical outcomes.

Histologic analysis of brains from human autopsy cases have shown that the density and distribution of neurofibrillary tangles (NFTs) correlate with cognitive decline in AD (*3,4*). Therefore, the measurement of changes in NFT density and distribution in vivo could provide a relevant pharmacodynamic biomarker for measuring disease progression. Measurement of a therapeutic intervention's ability to slow or halt NFT progression could enable early clinical decision making on the promise of novel disease-modifying mechanisms before investment in a large clinical outcomes trial. PET tracers can be useful for the noninvasive quantification of proteins; therefore, an NFT PET tracer is an attractive approach as a tool to quantify NFT pathology in vivo. Provided sufficient sensitivity to detect longitudinal changes can be demonstrated, an NFT PET tracer has the potential to provide a critical disease-relevant tool for quantifying a stabilization or changes in NFT formation for investigational disease-modifying therapeutics of AD.

Several radioligands generally referred to as tau PET tracers but predominantly characterized in NFT-rich AD brain tissue and AD patients have been reported and reviewed in recent literature (Fig. 1) (*5,6*). ^{18}F-AV-1451 (^{18}F-T807) was the first PET tracer to show promise for quantifying NFT pathology in AD patients (*7*) and is currently the most widely studied NFT PET tracer. However, it is

Received Feb. 1, 2016; revision accepted Apr. 11, 2016.
For correspondence or reprints contact: Eric D. Hostetler, Merck & Co., Inc., 770 Sumneytown Pike, WP44D-2, West Point, PA 19486-0004.
E-mail: eric.hostetler@merck.com
Published online May 26, 2016.

not clear if the reported signal in mild cognitive impairment subjects and early AD patients is sufficient for robust detection of longitudinal changes. Additionally, the specific signal continues to increase throughout the duration of the PET scan in mild cognitive impairment and AD patients (*7*), making reliable quantification challenging for this tracer. Furthermore, ^{18}F-AV-1451 shows high-affinity off-target binding (*8,9*), which creates uncertainty in the interpretation of changes in tracer signal over time. ^{18}F-T808 is a high-affinity, selective PET tracer for NFTs that showed promising initial results in human PET studies, but further evaluation has not been reported (*10*). Multiple ^{18}F-labeled NFT PET tracers have been evaluated by investigators at Tohoku University (*5*), the most recent being ^{18}F-THK5351, which has shown increased binding in the cortical regions of AD patients but also shows off-target binding in the basal ganglia (*11*). ^{11}C-PBB3 has been shown to provide a specific signal in AD patients that is differentiated from amyloid plaque PET tracer binding patterns (*12*). Our goal was to develop an ^{18}F-labeled PET tracer with superior selectivity, sensitivity, and in vivo kinetic behavior for the purposes of patient identification and longitudinal quantification of NFTs in human AD brain; the preclinical characterization of the NFT PET tracer ^{18}F-MK-6240 is described herein.

MATERIALS AND METHODS

General

^{18}F-fluoride was produced by PETNET pharmaceuticals using a Siemens RDS-111 cyclotron. A target containing ^{18}O-H_2O was irradiated with an 11-MeV proton beam, generating ^{18}F-fluoride. The ^{18}F-fluoride was trapped on an ion exchange resin and delivered in a lead-shielded container. AV-1451, ^{18}F-AV-1451, ^{3}H-AV-1451, ^{3}H-NFT-355, MK-6240 (6-(fluoro)-3-(1H-pyrrolo[2,3-c]pyridin-1-yl)isoquinolin-5-amine), ^{3}H-MK-6240, *N*-[(tert-butoxy)carbonyl]-*N*-(6-nitro-3-[1H-pyrrolo[2,3-c]pyridin-1-yl]isoquinolin-5-yl)carbamate, and ^{18}F-MK-6240 were prepared at Merck Research Laboratories (*13,14*). All other reagents and solvents were obtained from either Fisher Scientific or Aldrich. Radiochemical procedures were carried out remotely in a lead hot cell using a modified 233XL liquid handler (Gilson Inc.) (*15*). PET tracer identity, radiochemical purity, and specific activity were determined by evaluation on a Agilent 1100 LC system (Agilent Technologies) equipped with a Flow-Count photodiode radiodetector (Bioscan Inc.). The product was purified using a Gemini C6-Phenyl 250 × 10 mm, 5 μM HPLC column (Phenomex) at a flow rate of 4 mL/min. The mobile phase was 25% EtOH/75% NaOAc (10 mM, pH 4). The final preparation was tested for chemical and radiochemical purity by means of an analytical HPLC system (Agilent) using an XBridge Phenyl 3.5 μm 4.6 × 150 mm column (Waters) at a flow rate of 1.0 mL/min. The mobile phase was 20% acetonitrile/80% sodium acetate (10 mM, pH 4). ^{18}F-MK-6240 concentration was determined by means of an ultraviolet detector (254 nm). Confirmation of the identity of the product was determined by coinjection of a sample of MK-6240, and radiochemical purity was determined using a sodium iodide detector (Bioscan). Radiochemical purity was calculated from the percentage radioactivity attributed to isolated peak in the radioactive HPLC trace after integration of all radioactive peaks. The specific activity (GBq/μmol) of the radioligand was determined by withdrawing an aliquot (0.1 mL) of the preparation, determining the amount of radioactivity in a dose-calibrator, and correcting for decay from end of synthesis. The aliquot was evaluated by HPLC, and the ultraviolet response was compared against a calibration curve that was prepared with the unlabeled reference standard to determine the mass associated with the decay-corrected radioactivity of the injected aliquot.

Binding Affinity Measurements: Radioligand Competition Binding Assay

NFT Binding Assay. K_i inhibitory constant measurements for test compounds were carried out by equilibrium binding of ^{3}H-NFT-355 (K_d ~0.3 nM) in the presence of various concentrations of unlabeled test compound. Briefly, 250-μL solutions containing 0.5 mg/mL NFT-enriched brain homogenate (AD brain frontal cortex), 0.3 nM ^{3}H-NFT-355, and various concentrations of unlabeled test compound in assay buffer (phosphate-buffered saline [PBS] containing 0.1 mg/mL bovine serum albumin [BSA]) were incubated for 90 min in a 96-well deep well plate at room temperature with gentle shaking. Bound ligand was separated from free ligand by rapid filtration and washings using a GF/C filter plate (presoaked in 0.2% PEI) and FilterMate harvester (Perkin Elmer). Plates were washed using cold buffer solution (5 mM Tris-HCL, pH 7.4). The filter plate was dried, and 50 μL of scintillation liquid (Microscint-20; Perkin Elmer) were added to each well. Signal from bound radioligand was read using a TopCount scintillation counter (Perkin Elmer). Nonspecific binding was assessed by measuring radioligand binding in the presence of a high concentration (1 μM) of unlabeled, structurally diverse compound binding to the same (specific) target site. Half-maximal inhibitory concentration (IC_{50}) was estimated by fitting the data to a nonlinear 4-parameter logistic fit based on the Levenberg–Marquardt algorithm. K_i was calculated from the IC_{50} value using the Cheng–Prusoff equation (*16*).

Amyloid-β Binding Assay. K_i measurements for test compounds were carried out by equilibrium binding of a single concentration of ^{3}H-MK-3328, a radioligand with high affinity for amyloid-β (*17*), in the presence of various concentrations of unlabeled test compound. Briefly, 250-μL solutions containing amyloid-β–enriched brain homogenate (0.7 mg/mL) (AD brain frontal cortex), 2 nM ^{3}H-MK-3328, and various concentrations of unlabeled test compound in assay buffer were incubated for 90 min in 96-well deep-well plates at room temperature with gentle shaking. Subsequent steps and data analysis were as described above for the NFT binding assay.

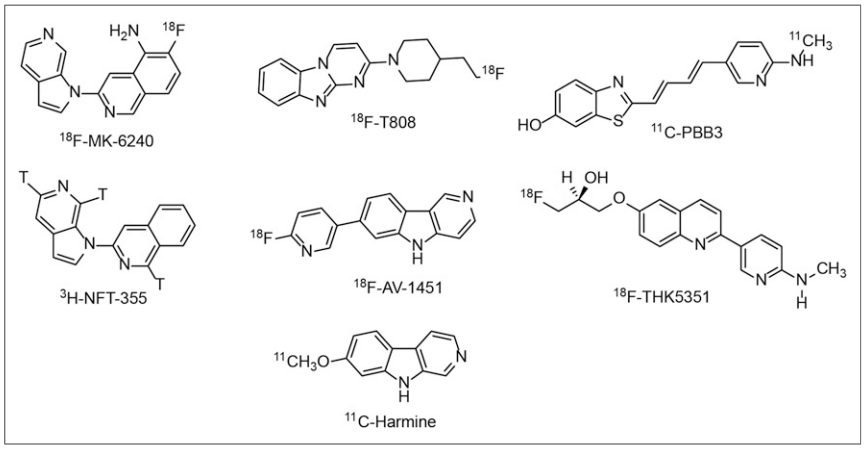

FIGURE 1. Structures of NFT ligands ^{18}F-MK-6240, ^{18}F-T808, ^{11}C-PBB3, ^{3}H-NFT-355, ^{18}F-AV-1451, and ^{18}F-THK5351 and structure of the MAO-A ligand ^{11}C-harmine.

In Vitro Brain Tissue Homogenate Binding Studies

Determination of K_d in Human Brain Tissue Homogenates. Hot saturation binding assays using ^{3}H-MK-6240 were performed using human brain cortex homogenates. Crude homogenates (2 mg/mL of wet tissue

weight) were preincubated in Skatron tube strips (SK15776) with dimethyl sulfoxide or unlabeled competing compound at room temperature for 30 min in assay buffer (PBS + 0.1 % BSA). The concentrations of unlabeled competing compounds used to define nondisplaceable binding (NDB) were 1 μM unlabeled MK-6240 or 0.5 μM T-808. Various concentrations of ^{3}H-MK-6240 were added to the assay tubes. The final assay volume after addition of all components was 0.25 mL per tube, and the final dimethyl sulfoxide concentration was 2%. The components of the assay in the tubes were mixed by brief vortex, and the assay tubes were incubated at 37°C for 90 min. Following incubation, the reaction mixtures were transferred onto Skatron GF/C filters (SK11731) pretreated with 0.1% BSA (Sigma A-7030), by a Skatron Combi cell harvester, and promptly washed with ice-cold PBS on setting 3-3-3. The filters were transferred to Pico Pro vials (Perkin Elmer), 2 mL of Ultima Gold (Perkin Elmer) scintillation cocktail were added per vial, and the vials were allowed to sit at room temperature for more than 3 h before scintillation counting using a Perkin Elmer Tri-Carb 2900TR for 1 min for disintegration per min (dpm). All data were fit to a 1-site binding model using Prism software (GraphPad). Competition of ^{3}H-MK-6240 binding by AV-1451 was evaluated by adding different concentrations of unlabeled AV-1451 in ^{3}H-MK-6240 hot saturation binding assays. For binding assays using ^{3}H-AV-1451, the procedures were similar to those of ^{3}H-MK-6240 binding assays, except using 1 μM of unlabeled AV-1451 or 0.5 μM of T808 to define NDB.

Competition Binding Assays Using ^{3}H-AV-1451. Displacement binding assay using ^{3}H-AV-1451 was carried out in non-AD human brain cortex homogenates. Brain homogenates at 2 mg/mL were first incubated in PBS assay buffer containing 0.1% BSA at room temperature for 30 min. Then, ^{3}H-AV-1451 (3 nM) and various concentrations of competing compounds, including clorgyline, MK-6240, and self-block, were added into each assay tube separately in triplicates. The assay tubes were gently mixed by brief vortex and incubated for 90 min at room temperature. Following incubation, filtration procedures were used to separate unbound radioligand from bound in each assay tube as described in the ^{3}H-MK-6240 binding assay. NDB was defined using 1 μM of unlabeled clorgyline. The filters collected from filtration procedures were counted in a liquid scintillation counter (Tri-Carb 2900TR; Perkin Elmer) for 1 min for radioactivity (dpm). The data were analyzed by a 1-site competition model using Prism software.

In Vitro Autoradiography

Autoradiography with ^{3}H-MK-6240 in human brain slices was performed similarly to previously reported methods (*18*). Briefly, brain slices were first preincubated for 15 min at room temperature in assay buffer (PBS, pH 7.5), containing 0.1% BSA but no radioligand. Then, the slices were placed into incubation assay buffer containing either ^{3}H-MK-6240 (0.3 nM) or ^{3}H-AV-1451 (2 nM) and incubated at room temperature for 90 min. Following incubation, the slices were washed in ice-cold wash buffer (PBS, pH 7.5) 3 times with 3 min per wash, and then rinsed in ice-cold distilled water for 5 s. The slices were dried at room temperature by air blower and placed into a cassette against a FUJI phosphorimaging plate (TR-2025). After 7-d exposure at room temperature, the phosphor imaging plate was scanned using a FUJI BAS5000 scanner. The scanned images were analyzed using MCID 7.0 software (GE Healthcare). NDB was defined by incubation with T808 (500 nM) or self-block (50 nM for MK-6240 and 200 nM for AV-1451).

Immunohistochemistry

Human brain sections were fixed in cold acetone/ethanol and washed in PBS/0.1% Tween (PBST). After blocking of endogenous peroxidases, the sections were incubated overnight at 4°C with either mouse anti-AT8 (MN1020; Fisher Scientific) or mouse anti-Beta amyloid 6E10 (SIG-39320; Biolegend). Sections were washed in PBST and incubated with horseradish peroxidase–conjugated anti-mouse/rat IgG (H+L) polymer (IH-8061; ImmunoBioScience Corp.). Sections were washed again in PBST, incubated with 3,3' diaminobenzidine chromagen, and then counterstained with hematoxylin.

Lipophilicity Measurement

The partition coefficient (log D) was determined by partitioning the compound of interest between octanol and phosphate buffer at pH 7.4 and measuring the concentration of compound in each layer.

Transport in P-Glycoprotein (P-gp)–Transfected Cell Lines

The P-gp transport ratio, that is, the ratio of permeabilities across each direction of the cell monolayer, for MK-6240 was evaluated across monolayers of porcine renal epithelial cells overexpressing human P-gp (*19*). Verapamil, a known P-gp substrate, was evaluated as a positive control.

Radiochemistry

Synthesis of ^{18}F-MK-6240. After its concentration on an anion exchange resin, ^{18}F-fluoride was eluted using a solution consisting of K_2CO_3 (2.1 mg), K_{222} (7 mg), water (0.07 mL), and acetonitrile (0.63 mL) into a borosilicate V-shaped vial (1.5 mL) stationed in a microwave cavity. Solvents were evaporated at 110°C (45W) using an argon stream. ^{18}F-fluoride was further dried by using 2 consecutive additions and evaporation of acetonitrile (0.5 mL). After being cooled, *N*-[(tert-butoxy)carbonyl]-*N*-(6-nitro-3-[1H-pyrrolo[2,3-c]pyridin-1-yl]isoquinolin-5-yl)carbamate (0.3-2 mg) in dimethyl formamide (0.3 mL) was added, the reaction vessel was sealed, and the mixture was heated using microwaves as follows: 90°C (45 W) for 3 min, then 110°C (45 W) for 3 min, then 120°C (75 W) for 3 min, then 140°C (75 W) for 3 min. The reaction was then quenched with NaOAc (0.700 μL, 10 mM, pH 4) and heated at 100°C (45W) for 120 s. The reaction mixture was cooled to 70°C, and water (0.5 mL) was added to the mixture prior to injection onto a semiprep high-performance liquid chromatography (HPLC) column. The fraction containing ^{18}F-MK-6240 (21–22 min) was collected in a heated pear-shaped flask, evaporated under negative pressure, diluted with 0.9% sterile saline solution (6 mL), and transferred into a sterile vial to yield 3.18 GBq of ^{18}F-MK-6240 with a specific activity of 91.8 GBq·μmol^{-1} and a radiochemical purity of greater than 98%.

Synthesis of ^{3}H-MK-6240. ^{3}H-MK-6240 was prepared by metal-catalyzed tritium exchange (4.4 mg of Rh; 0.9 mg of MK-6240, 250 mm Hg T2, THF, 16 h) on a Tri-Sorber Tritiation Manifold (LabLogic Systems Ltd.) followed by preparative HPLC purification (99.8% radiochemical purity, 204 MBq, 1.0 GBq/μmol).

Animals

All monkey PET imaging studies were conducted under the guiding principles of the American Physiological Society and the Guide for the Care and Use of Laboratory Animals published by the U.S. National Institutes of Health (*20*) and were approved by the West Point Institutional Animal Care and Use Committee at Merck Research Laboratories. Rhesus monkeys (male, ~10 kg, $n = 4$) were initially sedated with ketamine (10 mg/kg, intramuscularly), then induced with propofol (5 mg/kg, intravenously), intubated, and respired with medical-grade air and oxygen mixture at approximately 10 mL·breath^{-1}kg^{-1} and 23 respirations per min. The anesthesia was maintained with propofol (0.4–0.55 mg·kg^{-1}·min^{-1}) for the duration of the study. Body temperature was maintained with circulating water heating pads, and temperature, oxygen saturation, blood pressure, and end-tidal CO_2 were monitored for the duration of the study.

Imaging Procedure

PET scans were obtained on an ECAT EXACT HR+ or a Biograph PET/CT (Siemens Healthcare) in 3-dimensional mode; transmission data for attenuation correction were acquired in 2-dimensional mode

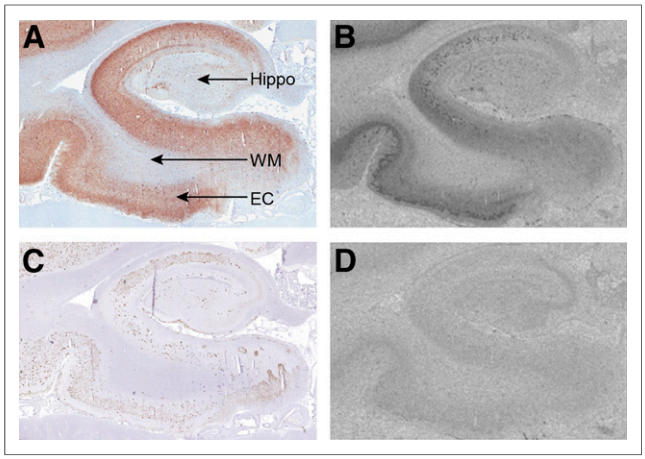

FIGURE 2. Results from autoradiography studies with ^{3}H-MK-6240 in entorhinal cortex (EC) and hippocampus (Hippo) of an NFT-rich AD brain donor. (A) AT8 immunohistochemical staining for phospho-tau. (B) ^{3}H-MK-6240 total binding. (C) 6E10 staining for amyloid plaque. (D) ^{3}H-MK-6240 in presence of 500 nM T808. WM = white matter.

before injection of the radiopharmaceutical. Dynamic emission scans were obtained for 90–120 min following a 2-min intravenous bolus injection of the respective PET tracer (~185 MBq). Data were reconstructed using a 3-dimensional ordered-subset expectation maximization iterative algorithm with 6 iterations and 16 subsets and an all-pass ramp filter. Monkeys were scanned on a Siemens Trio 3T magnet to obtain anatomic MR images.

Baseline PET scans with ^{18}F-MK-6240 and ^{18}F-AV-1451 were acquired in 3 rhesus monkeys. For the self-block PET studies, monkeys were dosed with unlabeled AV-1451 (intravenously, 0.5 or 1.5 mg/kg in 30% aqueous Captisol; Ligand Pharmaceuticals) 30 min prior to administration of ^{18}F-AV-1451. The same monkeys were dosed with unlabeled MK-6240 (intravenously, 0.5 mg/kg in 30% aqueous Captisol) 30 min prior to administration of ^{18}F-MK-6240 in a separate PET study. Metabolite-corrected input functions were obtained in all PET studies from the measurement of total radioactivity in arterial plasma with correction for radioactive metabolites as determined by HPLC analysis.

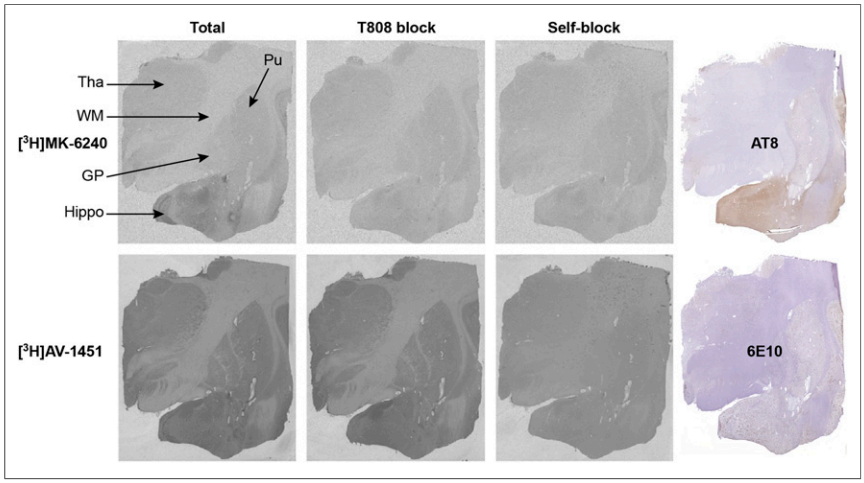

FIGURE 3. Autoradiography of ^{3}H-MK-6240 and ^{3}H-AV-1451 in subcortical regions of NFT-rich AD brain donor and immunostaining for phosphorylated tau (AT8) and amyloid-β-(6E10). GP = globus pallidus; Hippo = hippocampus; Pu = putamen; Tha = thalamus; WM = white matter.

Image Analysis and Quantification

PET data were corrected for isotope decay, attenuation, scatter, and dead-time using the software provided by the scanner manufacturer. The image processing, generation of time activities, and compartmental modeling were performed using in-house analysis software developed in Matlab (The MathWorks, Inc.) and the SPM8 toolbox (http://www.fil.ion.ucl.ac.uk/spm). Briefly, dynamic PET datasets were used to generate an average PET image (motion correction was performed prior to averaging, if required) that was rigidly registered to the corresponding T1 MR image using mutual information as the cost function followed by the nonlinear registration of a rhesus MRI template, and the corresponding atlas, to the individual's MRI. Visual assessment was performed for each registration. Regional time–activity curves were generated by applying the registered rhesus atlas to the dynamic PET data. Time–activity curves were normalized for injected activity and subject's weight (SUV) for display. Regional volumes of distribution (V_T) were determined by fitting a 2-compartment model (the most parsimonious model that described the data appropriately) using an arterial input function, which represents the radioactivity arterial plasma concentration of the parent tracer (^{18}F-MK-6240 or ^{18}F-AV-1451). A 5% blood volume component was assumed in the models.

RESULTS

MK-6240 displayed high affinity (K_i = 0.36 ± 0.8 nM [n = 8]) in NFT-rich AD brain homogenates versus the selective, high-affinity NFT ligand ^{3}H-NFT-355. MK-6240 bound poorly to amyloid plaques, with a K_i of 10 μM versus the amyloid plaque ligand ^{3}H-MK-3328 in plaque-rich AD brain homogenates. MK-6240 showed no significant activity in a panel of 118 commonly screened proteins in the central nervous system, with an IC_{50} of greater than 1 μM for all targets. The logD of MK-6240 was moderate at 3.32. MK-6240 showed high cell permeability (29×10^{-6} cm/s) and was not a substrate for the P-gp efflux pump (BA/AB ratio = 1.3 at a test concentration of 0.1 μM).

^{3}H-MK-6240 showed a large amount of displaceable binding in the gray matter of the entorhinal cortex and hippocampus of NFT-rich human AD brain slices, with no displaceable binding in the adjacent white matter (Figs. 2B and 2D). The pattern of ^{3}H-MK-6240 binding compared (Fig. 2B) favorably with phospho-tau immunostaining (Fig. 2A) and but not with amyloid-β-immunostaining (Fig. 2C). ^{3}H-MK-6240 binding was displaced using the NFT-selective ligand T808 (Fig. 2D).

In subcortical regions of AD brain, ^{3}H-MK-6240 displayed strong binding in the hippocampus, which was displaced to similar levels of NDB by either T808 or self-block, indicating high selectivity for binding NFTs (Fig. 3). ^{3}H-MK-6240 showed no apparent displaceable binding in neighboring NFT-poor subcortical regions (thalamus, putamen, globus pallidus). Compared with ^{3}H-MK-6240, ^{3}H-AV-1451 showed a smaller displaceable binding signal in the hippocampus. In all neighboring subcortical regions, ^{3}H-AV-1451 showed binding that was not displaced by the NFT-selective ligand T808 but was displaced by self-block, suggestive of off-target binding to non-NFT

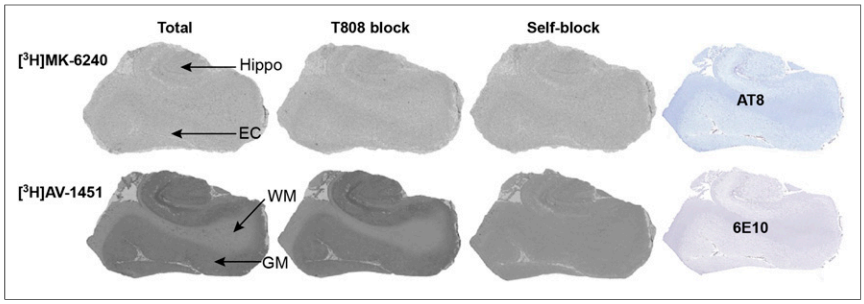

FIGURE 4. Autoradiography of ^{3}H-MK-6240 and ^{3}H-AV-1451 in entorhinal cortex/hippocampus of elderly non-AD brain donor and immunostaining for phosphorylated tau (AT8) and amyloid-β-(6E10). EC= entorhinal cortex; GM = gray matter; Hippo = hippocampus; WM = white matter.

sites (Fig. 3). The pattern of ^{3}H-MK-6240 binding compared favorably with AT8 immunostaining for phospho-tau (Fig. 3).

In non-AD brain slices characterized to have negligible levels of NFTs and amyloid plaques, ^{3}H-MK-6240 displayed negligible displaceable binding density under total binding and block conditions (Fig. 4). ^{3}H-AV-1451 showed strong displaceable binding in the entorhinal cortex and hippocampus of non-AD brains that was only blocked by self, not by T808, suggesting the ^{3}H-AV-1451 displaceable binding in non-AD brains was not related to binding NFTs (Fig. 4).

In NFT-rich AD brain tissue homogenates, saturation binding studies showed ^{3}H-MK-6240 has a subnanomolar K_d for NFTs. This resulted in a 2- to 5-fold-higher B_{max}/K_d (concentration of available binding sites and equilibrium dissociation constant, respectively) ratio for ^{3}H-MK-6240 than ^{3}H-AV-1451 as evaluated in either frontal cortex or entorhinal cortex of 5 different AD brain donors with varying levels of NFT pathology (Table 1). The K_d of ^{3}H-MK-6240 was similar (0.26 ± 0.08 nM, $n = 5$) across a range of NFT densities (B_{max}). As expected, the percentage of radioactivity that was nondisplaceable generally decreased as the B_{max} increased. ^{3}H-MK-6240 showed relatively low NDB at K_d concentrations (Table 1), a favorable characteristic for in vivo imaging.

In non-AD cortical brain homogenates from 3 different brain donors confirmed to have negligible amounts of NFTs by AT8 immunohistochemistry, saturation binding studies using self-block to define NDB indicated that ^{3}H-MK-6240 showed no displaceable binding non-AD brain donors (Table 2). In these same pools of brain tissue homogenate, ^{3}H-AV-1451 showed high-affinity, displaceable binding (Table 2). A representative saturation binding curve for ^{3}H-MK-6240 and ^{3}H-AV-1451 in 1 non-AD donor are shown in Supplemental Figures 1A and 1B (supplemental materials are available at http://jnm.snmjournals.org), respectively. Titration of ^{3}H-AV-1451 with the monoamine oxidase A (MAO-A) inhibitor clorgyline resulted in complete, high-affinity (K_i = 0.43 nM) displacement of ^{3}H-AV-1451 (Supplemental Fig. 1C), suggesting that the displaceable binding observed with ^{3}H-AV-1451 in non-AD brain tissues was due to MAO-A binding.

^{3}H-MK-6240 bound to the same NFT binding site as AV-1451 in NFT-rich brain homogenates. Saturation binding studies with ^{3}H-MK-6240 were performed in the presence of different fixed concentrations of AV-1451. The presence of unlabeled AV-1451 increased the apparent K_d of ^{3}H-MK-6240 linearly with increasing concentration of AV-1451 (Supplemental Fig. 1D), as expected for compounds that compete for the same binding site. Furthermore, nonlinear curve fitting of ^{3}H-MK-6240 saturation binding data indicated that MK-6240 bound to a single site. Because both MK-6240 and AV-1451 bind to the same site, it is unlikely that MK-6240 will bind to tau aggregates found in non-AD tauopathies based on the recent report (*8*) indicating AV-1451 does not bind tau aggregates found in non-AD tauopathies. Future studies will be needed to confirm this hypothesis.

The incorporation of ^{18}F to provide ^{18}F-MK-6240 was accomplished by nucleophilic displacement of a nitro group with ^{18}F-KF on a bis-Boc protected precursor, followed by heating with sodium acetate to reveal the aniline group. After HPLC purification, ^{18}F-MK-6240 was isolated with high purity (>98%) and specific activity (>90 GBq·μmol^{-1}) and in good radiochemical yield. PET studies in rhesus monkeys showed that ^{18}F-MK-6240 had favorable pharmacokinetic properties, distributing rapidly across the blood–brain barrier, followed by rapid clearance (Fig. 5A). Distribution was homogeneous across all brain regions, as expected because tau pathology was not present in the monkey brain (Fig. 5B). Some defluorination was observed, which manifested as skull uptake, plateauing at approximately 1 SUV within the first several minutes of the PET scan.

Self-block PET studies with ^{18}F-MK-6240 in the rhesus monkey were performed by injecting a high dose of unlabeled MK-6240

TABLE 1
B_{max} and K_d Values for ^{3}H-AV-1451 and ^{3}H-MK-6240 Binding in NFT-rich AD Brain Tissues

	^{3}H-AV-1451				^{3}H-MK-6240			
Donor tissue	B_{max} (nM)	K_d (nM)	B_{max}/K_d	% NDB at K_d	B_{max} (nM)	K_d (nM)	B_{max}/K_d	% NDB at K_d
AD507 entorhinal cortex	15.0	1.4	11	88	7.8	0.14	56	33
AD906 entorhinal cortex	62.5	3.72	17	78	18.8	0.30	63	30
AD111 frontal cortex	67.0	1.70	39	68	35.9	0.25	144	19
AD790 frontal cortex	46.9	0.63	74	55	39.3	0.24	164	24
AD106 frontal cortex	119.7	1.10	109	36	93.4	0.38	246	12

NDB was defined by T808.

TABLE 2
B_{max} and K_d Values for ^{3}H-AV-1451 and ^{3}H-MK-6240 Binding in Non-AD Brain Tissues

Donor tissue	^{3}H-AV-1451			^{3}H-MK-6240		
	B_{max} (nM)	K_d (nM)	B_{max}/K_d	B_{max} (nM)	K_d (nM)	B_{max}/K_d
Non-AD037 frontal cortex	61	10.3	5.9	Nonsaturable	Nonsaturable	Nonsaturable
Non-AD294 frontal cortex	152	4.94	31	Nonsaturable	Nonsaturable	Nonsaturable
Non-AD449 frontal cortex	190	4.79	40	Nonsaturable	Nonsaturable	Nonsaturable

NDB was defined by self-block.

before tracer injection. No difference in total V_T was observed between the baseline and self-block PET studies (Fig. 6A). In contrast, ^{18}F-AV-1451 self-block PET studies in monkeys showed a marked reduction in V_T between baseline and self-block (Fig. 6B). This result is indicative of off-target binding and is consistent with the high-affinity binding observed by ^{3}H-AV-1451 in non-AD brain.

DISCUSSION

To date, no published NFT PET tracers have been validated to bind tau pathology from transgenic animal models with the same affinity as tau pathology from human AD. Therefore, potential candidates were screened for NFT binding affinity in cortical homogenates from AD cortex, which had been characterized by immunohistochemistry to be high in NFT density. These brain regions also contain high levels of amyloid plaque; therefore, the use of ^{3}H-NFT-355 (*14*), a radioligand that is highly selective for NFTs (K_i = 0.3 nM) versus amyloid plaque (K_i > 10 μM), was critical. To confirm compound selectivity for amyloid plaque, a counterscreen was conducted using the amyloid plaque tracer ^{3}H-MK-3328 (*21*) in AD brain homogenate characterized to be amyloid plaque–rich but NFT-poor. Use of these in vitro screens led to the identification of MK-6240, which displayed high affinity for NFTs and weak affinity for amyloid plaque. Additionally, MK-6240 showed favorably moderate lipophilicity (*22*), suggesting that NDB would be minimized, as well as good in vitro characteristics for crossing the blood–brain barrier (non–P-gp substrate, good cell permeability). Its high-affinity, selective binding for NFTs and excellent physicochemical properties warranted a more detailed characterization of MK-6240 as an NFT PET tracer candidate. Therefore, ^{3}H-MK-6240 was synthesized to enable detailed characterization of the ligand's binding characteristics in human brain tissue.

Because of the difficulty of differentially diagnosing AD from other dementias and mild cognitive impairment in the early stages of disease (*23*), it was important to build confidence that ^{18}F-MK-6240 has the potential for excellent sensitivity for NFTs in human subjects. Fortunately, the clinical success of ^{18}F-AV-1451 to image NFTs in human AD patients provided the opportunity to establish an in vitro benchmark for comparison to MK-6240 as we performed rigorous in vitro evaluation of the new tracer candidate. The sensitivity of MK-6240 binding for NFTs was evaluated by determining and comparing B_{max}/K_d ratios, which are proportional to the in vivo signal from a PET tracer (*24,25*), for MK-6240 and AV-1451 in NFT-rich cortical brain homogenates from 5 different AD brain donors. Consistent with its higher affinity, ^{3}H-MK-6240 showed a B_{max}/K_d ratio up to 5-fold higher than AV-1451 across different AD brain donors with a wide range of NFT densities (B_{max}) (Table 2). The B_{max} values for MK-6240 and AV-1451 binding sites in these experiments are lower than what has been reported for some other NFT PET ligands (THK-5117 (*26*)). This could be due to lower NFT density in the tissues evaluated in this study. An additional factor may be due to the use of T808, a selective and structurally dissimilar NFT ligand, to define NDB. The use of self-block to define NDB will result in a higher B_{max} if off-target binding sites of similar affinity are present. In fact, this is observed with AV-1451, which has a B_{max} approximately 2- to 5-fold higher when self-block is used to define NDB (data not shown). The excellent sensitivity of MK-6240 can also be seen in autoradiography studies, in which ^{3}H-MK-6240 showed a greater contrast of binding compared with AV-1451 in the hippocampus versus subcortical regions (Fig. 3).

The potential for MK-6240 off-target binding was evaluated by performing autoradiography and saturation binding studies in the entorhinal cortex/hippocampus of non-AD brain donors and by performing displacement PET studies in the monkey brain. AV-1451 showed high-affinity, displaceable binding in these studies despite the absence of phosphorylated tau in these tissues. The nature of this off-target binding has been reported to be associated with MAO-A (*9*). Our results concur with these findings, because the MAO-A inhibitor corgyline completely displaced ^{3}H-AV-1451 binding in non-AD brain tissue. In an early publication describing ^{18}F-AV-1451

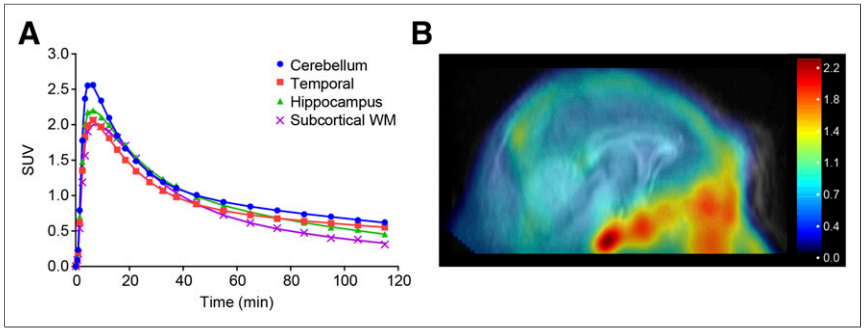

FIGURE 5. (A) ^{18}F-MK-6240 time–activity curves. (B) Summed PET image (40–80 min) of ^{18}F-MK-6240 in rhesus monkey brain overlaid on MR image; sagittal view. Scale is in SUV.

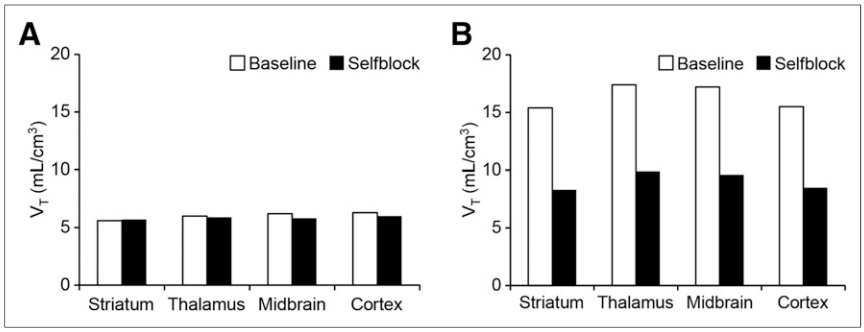

FIGURE 6. Comparison of total V_T in selected brain regions between baseline and self-block PET studies for ^{18}F-MK-6240 (A) and ^{18}F-AV-1451 (B) in same rhesus monkey. Plots are representative of results in 3 different monkeys.

(^{18}F-T807) (*27*), it was recognized that the structure of ^{18}F-AV-1451 showed close similarity to the reported MAO-A PET tracer ^{11}C-harmine (Fig. 1) (*28*). However, AV-1451 was found to have weak affinity (μM) for MAO-A in this early report (*27*). The reasons for the discrepancy in MAO-A binding between the initial report and recent observations are unknown. Nevertheless, if MAO-A enzyme availability changes due to age or other pharmacologic factors such as smoking (*29*), this could potentially confound the interpretation of longitudinal changes in the PET signal from ^{18}F-AV-1451. MK-6240, by comparison, showed no displaceable binding in analogous studies in non-AD brain tissue. Consistent with high selectivity for binding NFTs, autoradiography in NFT-rich AD brain slices indicated the blockade of ^{3}H-MK-6240 binding was similar using either T808 or self-block. These results provided clear evidence that MK-6240 has excellent selectivity for binding NFTs.

Monkey PET studies showed that ^{18}F-MK-6240 possessed favorable prerequisites for in vivo imaging. ^{18}F-MK-6240 rapidly achieved high levels of brain penetration with favorably rapid clearance. Distribution was homogeneous, as expected for a species with negligible levels of NFTs, and no increased white matter retention was observed, consistent with the favorably moderate lipophilicity of MK-6240. Kinetic analysis of the PET data revealed a V_T which stabilized after 90 min of imaging, suggesting that radiolabeled brain-penetrant metabolites are not present at significant levels. Furthermore, minimal differences in ^{18}F-MK-6240 V_T were observed between the baseline and self-block PET studies, suggesting that ^{18}F-MK-6240 does not possess high-affinity off-target binding to, for example, central nervous system receptors and enzymes that might provide a signal that confounds quantification of NFTs in human. Low levels of defluorination (radioactive uptake in the skull) were observed. In vitro metabolism studies in liver microsomes across species showed an oxidative defluorinated metabolite, which was less prominent in human microsomes as compared with the monkey: approximately 46% and 18% of MK-6240 remained in human and monkey, respectively, after a 15-min incubation in liver microsomes. The extent of defluorination in clinical studies will need to be carefully monitored to determine the impact of partial-volume effects of any tracer uptake in bone on quantifying changes in NFT signal in adjacent cortical regions.

CONCLUSION

^{3}H-MK-6240 displays high affinity and excellent selectivity for binding NFT-rich brain tissue as demonstrated by studies in postmortem tissue from AD and non-AD human brain donors. Further studies will be needed to determine whether MK-6240 binds to other forms of tau aggregates (e.g., coiled bodies, tufted astrocytes) observed in non-AD tauopathies. PET studies in rhesus monkeys indicate that ^{18}F-MK-6240 shows excellent in vivo characteristics, with rapid blood–brain barrier penetration and clearance, stable V_T, and homogeneous distribution throughout the brain. ^{18}F-MK-6240 is a promising PET tracer for in vivo quantification of NFTs and merits evaluation in human PET studies.

DISCLOSURE

The costs of publication of this article were defrayed in part by the payment of page charges. Therefore, and solely to indicate this fact, this article is hereby marked "advertisement" in accordance with 18 USC section 1734. MK-6240 is the subject of patent application WO2015191506A2. All authors were employees of Merck & Co., Inc. at the time of this work. No other potential conflict of interest relevant to this article was reported.

ACKNOWLEDGMENTS

We thank Jing Li for synthesis of *N*-[(tert-butoxy)carbonyl]-*N*-(6-nitro-3-[1H-pyrrolo[2,3-c]pyridin-1-yl]isoquinolin-5-yl)carbamate and MK-6240, Arie Struyk and Joel Schachter for helpful discussions, and PETNET pharmaceuticals for supplying ^{18}F-fluoride.

REFERENCES

1. Villain N, Chetelat G, Grassiot B, et al. Regional dynamics of amyloid-beta deposition in healthy elderly, mild cognitive impairment and Alzheimer's disease: a voxelwise PiB-PET longitudinal study. *Brain.* 2012;135:2126–2139.
2. Toledo JB, Xie SRX, Trojanowski JQ, Shaw LM. Longitudinal change in CSF tau and a-beta biomarkers for up to 48 months in ADNI. *Acta Neuropathol (Berl).* 2013;126:659–670.
3. Nelson PT, Alafuzoff I, Bigio EH, et al. Correlation of Alzheimer disease neuropathologic changes with cognitive status: a review of the literature. *J Neuropathol Exp Neurol.* 2012;71:362–381.
4. Bierer LM, Hof PR, Purohit DP, et al. Neocortical neurofibrillary tangles correlate with dementia severity in Alzheimers-disease. *Arch Neurol.* 1995;52:81–88.
5. Ariza M, Kolb HC, Moechars D, Rombouts F, Andres JI. Tau positron emission tomography (PET) imaging: past, present, and future. *J Med Chem.* 2015;58:4365–4382.
6. Shah M, Catafau AM. Molecular imaging insights into neurodegeneration: focus on tau PET radiotracers. *J Nucl Med.* 2014;55:871–874.
7. Chien DT, Bahri S, Szardenings AK, et al. Early clinical PET imaging results with the novel PHF-tau radioligand [F-18]-T807. *J Alzheimers Dis.* 2013;34:457–468.
8. Marquie M, Normandin MD, Vanderburg CR, et al. Validating novel tau PET tracer [F-18]-AV-1451 (T807) on postmortem brain tissue. *Ann Neurol.* 2015;78:787–800.
9. Vermeiren C, Mercier J, Viot D, et al. T807, a reported selective tau tracer, binds with nanomolar affinity to monoamine oxidase A. *Alzheimers Dement.* 2015;11:P283.
10. Chien DT, Szardenings AK, Bahri S, et al. Early clinical PET imaging results with the novel PHF-tau radioligand [F18]-T808. *J Alzheimers Dis.* 2014;38:171–184.
11. Harada R, Okamura N, Furumoto S, et al. F-18-THK5351: a novel PET radiotracer for imaging neurofibrillary pathology in Alzheimer disease. *J Nucl Med.* 2016;57:208–214.
12. Maruyama M, Shimada H, Suhara T, et al. Imaging of tau pathology in a tauopathy mouse model and in Alzheimer patients compared to normal controls. *Neuron.* 2013;79:1094–1108.

13. Walji AM, Hostetler ED, Greshock T, et al., inventors; Merck Sharp and Dohme Corp, assignee. Pyrrolo[2,3-C]pyridines as imaging agents for neurofibrilary tangles. International patent WO2015/191506A2. December 17, 2015.
14. Walji AM, Hostetler ED, Greshock T, et al., inventors; Merck Sharp and Dohme Corp, assignee. Pyrrolo[2,3-C]pyridines as imaging agents for neurofibrilary tangles. International patent WO2015/188368A1. December 17, 2015.
15. Hostetler ED, Hamill TG, Francis BE, Burns HD. A versatile, commercially available automated synthesizer for the development and production of PET radiotracers. *J Labelled Comp Radiopharm.* 2001;44:S1042–S1044.
16. Cheng Y, Prusoff WH. Relationship between the inhibition constant (K1) and the concentration of inhibitor which causes 50 per cent inhibition (I50) of an enzymatic reaction. *Biochem Pharmacol.* 1973;22:3099–3108.
17. Hostetler ED, Sanabria-Bohorquez S, Fan H, et al. [F-18]fluoroazabenzoxazoles as potential amyloid plaque PET tracers: synthesis and in vivo evaluation in rhesus monkey. *Nucl Med Biol.* 2011;38:1193–1203.
18. Hamill TG, Sato N, Jitsuoka M, et al. Histamine H3 inverse agonist PET tracers labelled with carbon-11 or fluorine-18. *Neuroimage.* 2008;41:T22–T22.
19. Yamazaki M, Neway WE, Ohe T, et al. In vitro substrate identification studies for P-glycoprotein-mediated transport: species difference and predictability of in vivo results. *J Pharmacol Exp Ther.* 2001;296:723–735.
20. National Research Council. *Guide for the Care and Use of Laboratory Animals: Eighth Edition*. Washington, D.C.: National Academies Press; 2011.
21. Hostetler ED, Sanabria-Bohorquez S, Fan H, et al. [F-18]fluoroazabenzoxazoles as potential amyloid plaque PET tracers: synthesis and in vivo evaluation in rhesus monkey. *Nucl Med Biol.* 2011;38:1193–1203.
22. Patel S, Gibson R. In vivo site-directed radiotracers: a mini-review. *Nucl Med Biol.* 2008;35:805–815.
23. Jicha GA, Abner EL, Schmitt FA, et al. Preclinical AD workgroup staging: pathological correlates and potential challenges. *Neurobiol Aging.* 2012;3:622.e1.
24. Mintun MA, Raichle ME, Kilbourn MR, Wooten GF, Welch MJ. A Quantitative model for the in vivo assessment of drug-binding sites with positron emission tomography. *Ann Neurol.* 1984;15:217–227.
25. Innis RB, Cunningham VJ, Delforge J, et al. Consensus nomenclature for in vivo imaging of reversibly binding radioligands. *J Cereb Blood Flow Metab.* 2007; 27:1533–1539.
26. Lemoine J, Saint-Aubert L, Marutle A, et al. Visualization of regional tau deposits using 3H-THK5117 in Alzheimer brain tissue. *Acta Neuropathal Commun.* 2015;3:40.
27. Xia CF, Arteaga J, Chen G, et al. [F-18]T807, a novel tau positron emission tomography imaging agent for Alzheimer's disease. *Alzheimers Dement.* 2013; 9:666–676.
28. Bergström M, Westerberg G, Langstrom B. C-11-harmine as a tracer for monoamine oxidase A (MAO-A): In vitro and in vivo studies. *Nucl Med Biol.* 1997; 24:287–293.
29. Fowler JS, Volkow ND, Wang GJ, et al. Brain monoamine oxidase A inhibition in cigarette smokers. *Proc Natl Acad Sci USA.* 1996;93:14065–14069.